Platonic solids bouncing on a vibrating plate

Torsten Trittel [1,2] Dmitry Puzyrev [2,3] and Ralf Stannarius [2,4]

[1]*Department of Engineering, Brandenburg University of Applied Sciences, D-14770 Brandenburg an der Havel, Germany*
[2]*MARS, Otto von Guericke University Magdeburg, D-39106 Magdeburg, Germany*
[3]*Department of Microgravity and Translational Regenerative Medicine, Otto von Guericke University Magdeburg, D-39106 Magdeburg, Germany*
[4]*Institute of Physics, Otto von Guericke University Magdeburg, D-39106 Magdeburg, Germany*

The energy transfer between bouncing particles and rigid boundaries during impacts is crucially influenced not only by restitution coefficients of the material but also by particle shapes. This is particularly important when such particles are mechanically agitated with vibrating plates. Inertial measurement units are able to measure all acceleration and rotational velocity components of an object and store these data for subsequent analysis. We employ them to measure the dynamics of cubes and icosahedra on vibrating plates to study the efficiency of energy transfer into the individual degrees of freedom (DOFs) of the excited object. The rotational DOFs turn out to be much less excited than the vertical translational motion. Most remarkably, there is only little difference between the two Platonic solids in both the absolute energies and the energy partition ratios.

I. INTRODUCTION

A. Mechanically excited multiparticle ensembles

Mechanical excitation of solid particles with a vibrating plate is of fundamental practical importance in a number of industrial applications. For example, this technique can be used to supply kinetic energy to particle ensembles to fluidize a granular bed by shaking the container, and it is a standard excitation technique in statistical experiments with granular gases; see, e.g., Refs. [1–3]. These ensembles of freely flying macroscopic particles are intrinsically dissipative because of the inelastic collisions between individual constituents. A continuous excitation is needed if one wants to maintain a quasi-stationary dynamic state with constant total energy. In many previous experimental studies of three-dimensional (3D) granular gases, this energy input was realized by vibrating container walls (e.g., [4–10]). One of the important questions in such studies of vibration-excited granular materials is the input and distribution of kinetic energies among the particles and among the individual degrees of freedom (e.g., [10–21]). The energy partition is governed by two processes: the efficiency of energy entry into the system by contacts of particles with the vibrating container walls, and the redistribution of this energy in particle-particle interactions.

B. Observation techniques

One of the major difficulties of dynamical experiments with such multiparticle systems is the recording of the full dynamics of the individual objects, both translational and rotational motions. The classical approach is optical observation with either a single video camera (where the 3D information is lost) or stereoscopic observation with two or more cameras. This optical technique has two problems. First, it usually limits the experiments to very low particle number densities or shallow layers, because coverage of background

particles can seriously frustrate optical tracking. Second, the evaluation of positions from different views is not trivial, and third, particle rotations may impose additional problems not only in the automatic detection of positions but also for the correct determination of rotation axes and angles. Alternative observation techniques like positron emission particle tracking [22] can track positions of single particles, but neither this technique can treat multiple particles at once nor is it sensitive to rotational motion. The technique introduced below is complementary to these approaches and may solve some of the open questions; in particular, it can record rotational states of particles, it works in dense systems, and it can easily detect collisions.

C. Objects bouncing on vibrating ground plates

The elementary agitation process for the mechanical excitation of granular gases and the fluidization of granular beds can be studied with a single particle bouncing from a vertically vibrating plate. This process was extensively investigated experimentally, analytically, and numerically, in order to understand the characteristics and efficiency of the energy input, e.g., in Refs. [23–28]. The history of studies of bouncing spheres on a vibrating table started already more than half a century ago with work by Zaslavski [29] and Holmes [30], followed by a large number of publications dealing with the question of whether the motion is regular in general or if it can be chaotic (e.g., Refs. [31–35]). In all these investigations, simple spherical particles were considered. There is only a limited amount of literature about nonspherical particles, including, e.g., dimers [36–41], trimers [38], and rods [27,28].

While nonspherical grains are closer to many natural systems and more realistic for most applications in industry, they complicate the description because of the coupling of rotational and translational motion during collisions of the particles. All experiments mentioned above were based upon

optical observation techniques, where the trajectories and states of rotation were extracted from simple or stereoscopic video footage.

The purpose of this study is twofold: First, we introduce an observation technique that does not require the complex processing of stereoscopic optical data but retrieves information about the state of motion directly from the particles, and, second, we study objects that deviate from sphere shape but are highly symmetric. We focus on regular polyhedra with highest possible symmetries, *viz.*, the Platonic solids. They represent the only shapes where all edges and all sides are geometrically equivalent. The five Platonic solids span a broad variety of shapes from the acute-angled, jagged tetrahedron to the much more rounded dodecahedron, but most importantly, all of them have an inertia tensor with spherical symmetry, so that the angular momentum $\vec{J}$ is always parallel to the angular velocity $\vec{\omega}$, and nutations are excluded. In contrast to spherical particles, collisions with a vibrating plate or other obstacles introduce a torque onto the object and change its rotational state, except in a very few special cases. Collisions can convert translational into rotational energy of the body and vice versa. This changes the character of the bouncing behavior with respect to spheres qualitatively.

D. Selection of the particle shapes and geometrical considerations

While spheres do not experience torques at normal impact on a vibrating plate, objects that deviate from sphere shape like the Platonic solids are in general subject to torques. We start with the hypothesis that these torques are larger on average when the deviation from sphere shape is larger. The "classical" definition of sphericity (similarity to a sphere) as the ratio of the surface of a sphere with the same volume to the surface of the polyhedron is not useful for our purpose. We are interested in parameters that may cause a stronger influence of collisions on the rotation state. For the highly symmetric shapes of Platonic solids with given volume and homogeneous mass density, we consider two criteria that influence the excitation of rotations. On the basis of these criteria, we selected two of the five shapes for our experiments (the tetrahedron had to be excluded for technical reasons):

(1) The torque exerted on the object at impact: When the particle hits the plate with a given velocity and mass, this torque will be related to the distance ℓ from the contact point to the perpendicular through the center of mass. The maximum distance $\ell_{\max}$ is given by the circumcircle radius R_F of the faces of the polyhedra.

(2) The moment of inertia I: If a given torque during impact changes the angular momentum, the latter will be related to an angular velocity ω that is inversely proportional to the unique eigenvalue I of the inertia tensor of the body.

The analytical computation of the collision scenarios for Platonic solids is beyond the scope of this paper, but one may use a simple model to evaluate the efficiency of torques during impact: We assume that a body hits the horizontal nonvibrating plate with a vertical velocity v_1 and no rotations, $\omega_1 = 0$. Further, we make the simplifying assumption that the collision is fully elastic (no dissipation of kinetic energy). Then we obtain (see the Appendix) the new velocity v_2 and the angular velocity ω_2 after the collision as a function of v_1, and also the resulting rotational energy as a function of the initial kinetic energy. This computation contains many simplifications. One obvious oversimplification is that often the objects in the experiment bounce twice before the center of mass moves upward again. In such "double collisions", the angular momentum generated in the first hit is partially compensated by the second one. Also, the distance ℓ differs for the individual jumps, and thus the efficiency of the excitation of rotations is statistically distributed. Nevertheless, the model gives some useful clues: For the icosahedron and the dodecahedron, the optimum distance ℓ_{opt} where the excitation of rotations is most efficient is close to R_f, the maximum possible value of ℓ. Namely, for these two shapes the ratios ℓ_{opt}/R_F are comparable, within 2% deviation around $\ell_{\mathrm{opt}}/R_F \approx 0.9$. Thus, only collisions where the bottom face is almost horizontal will give an optimal outcome in rotational energy. This means that for the icosahedron and the dodecahedron, most of the collisions will produce a much smaller rotational energy than the maximum possible. For the cube and the octahedron, the ratios ℓ_{opt}/R_F are also quite comparable to each other, within 3% deviation around $\ell_{\mathrm{opt}}/R_F \approx 0.56$. Here one may expect that distances ℓ close to the optimum ℓ_{opt} are probably more often reached in individual collisions, even though a detailed investigation is needed to recheck this statement. Nevertheless, one may draw the conclusion that from the viewpoint of this simplified model, the efficiency of the excitation of rotations is rather similar for dodecahedra and icosahedra, and we thus have restricted the experimental study to the icosahedron. In the same sense, because of the similarity of the geometrical results for cube and octahedron, only the cube was chosen from these two for experiments. The tetrahedron differs most of all Platonic solids from a sphere shape, and the comparably small moment of inertia supports fast rotations. It probably has the best geometrical conditions to obtain high rotational energies with a single impact, and it would certainly be an interesting candidate for the experiments presented here, yet it was not suitable for the available hardware: The integration of the electronic board into a tetrahedron requires much larger edge lengths because of the pointed vertices. It would have a much larger mass, which brings the shaker used here (see the following section) to its mechanical limits.

II. EXPERIMENTAL

A. Electromagnetic shaker system

The Platonic solids were excited with an electromagnetic shaker driven by a Fame Audio 8002 amplifier. This shaker was equipped with a flat circular aluminum platform with about 30 cm diameter and 1 cm thickness; see Fig. 1(a). Each experiment was performed with a single polyhedron. A shallow sidewall prevented the jumping Platonic solid from leaving the plate. The shaking frequency f_{pl} and amplitude A_{pl} of the platform can be set by a custom-made LABVIEW program. The platform position is described by the vertical coordinate $z_{\mathrm{pl}}(t) = A_{\mathrm{pl}} \sin \omega_{\mathrm{pl}} t$ with $\omega_{\mathrm{pl}} = 2\pi f_{\mathrm{pl}}$. During shaking, the excitation was monitored with an accelerometer mounted at the plate. Our combination of shaker and amplifier was limited to a maximum plate acceleration $\Gamma = A_{\mathrm{pl}} \omega_{\mathrm{pl}}^2 \leqslant$
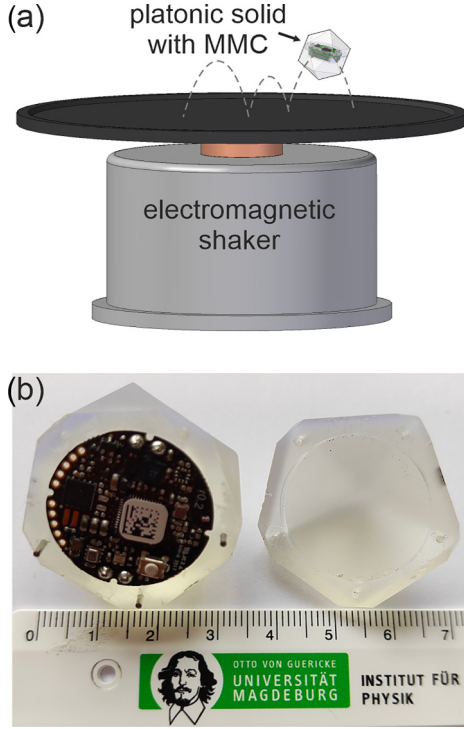
FIG. 1. (a) Sketch of the experimental equipment. The excitation is realized by an electromagnetic shaker. The Platonic solids are equipped with an autonomous inertial measurement unit (IMU) board, the MetaMotionC (MMC) from MBIENTLAB, to monitor the rotation of the bodies and the jump times (time between two consecutive plate contacts). The shaker platform (black) has a diameter of approximately 30 cm. The side wall at the circumference of the shaker plate is not shown. (b) Image of the two parts of the 3D printed icosahedron. The part shown on the left hosts the board.

$5\,g$ (gravitational acceleration $g = 9.81$ m/s^2). In all experiments reported here, we chose the maximum acceleration $\Gamma = 5\,g$ to reach long jump times t_j (time between two consecutive contacts of plate and jumping body) and heights. The corresponding combinations of frequency f_{pl} and amplitude A_{pl} can be found in Table I.

B. Platonic solids

We selected two different Platonic solids for the experiments, a cube and an icosahedron. Both were printed with a Form 2 SLA 3D printer with the suitable clear resin v4. The cured material has an ultimate tensile strength of 65 MPa and a tensile modulus of 2.8 GPa, so it is similar to acrylic glass

TABLE I. Frequency, amplitude, and maximum plate velocity for experiments in this study. Each object was excited by the electromagnetic shaker system for a few minutes using these parameters. The maximum plate acceleration was $\Gamma = 5\,g$ in all experiments.

Experiment no.	1	2	3	4
Frequency f_{pl} [Hz]	20	30	40	50
Amplitude A_{pl} [mm]	3.11	1.38	0.78	0.5
Maximum plate velocity V_{pl} [m/s]	0.39	0.26	0.195	0.156

TABLE II. Physical parameters of the two Platonic solids.

Platonic solid	Side length a [mm]	Mass m [g]	Moment of inertia I_{ps} [g cm^2]
Cube	26	22.04	24.83
Icosahedron	20.4	22.07	24.04

(polymethyl methacrylate). Each body consists of two parts that are glued together with the aid of aligning pins. Within the bodies are cutouts to equip them with the autonomous inertial measurement units (IMUs), shown in Fig. 1(b). The cutout is positioned such that the center of mass of the complete particle coincides with its geometrical center. Physical properties of these Platonic solids are given in Table II. Interestingly, these two objects have not only similar masses but also almost the same moments of inertia.

C. Smart inertial measurement units

In order to record the body motion, the Platonic solids were equipped with an autonomous IMU, the MetaMotionC (MMC) from MBIENTLAB. This chip allows one to monitor the rotations of the body around the body-fixed x, y, and z axes (up to $\pm 2000°$/s) and the linear accelerations in x, y, and z directions (up to $\pm 16\,g$) with a rate of 800 samples per second. To reach this sample rate, the chip is used in the onboard storage mode. We recorded the body motion for a few hundred seconds, so that each data set consists of several thousand individual jumps. The reconstruction of the exact trajectories from the accelerometer and gyroscope data may be possible in principle but was not attempted here. For simplicity, we used the accelerometer data to detect the contacts of the Platonic solid with the plate. These contacts appear as strong peaks in the acceleration data. During the free-flight phase, the recorded acceleration data are practically zero. From the peaks, we retrieve the jump times t_j and the corresponding upward particle velocity v_0 at the beginning of each individual jump, given by

$$v_0 = \frac{g}{2}t_j + \frac{\Delta z_{\mathrm{pl}}}{t_j}. \tag{1}$$

Here g is the gravitational acceleration and Δz_{pl} is the height difference of the shaker plate between the end and the start of each jump. The angular velocity $\vec{\omega}$ representing the three rotational degrees of freedom can be directly taken from the stored chip data. From the velocity v_0 and rotation rate we obtain both the translational energy in the vertical z direction,

$$E_z = \tfrac{1}{2}mv_0^2, \tag{2}$$

and the rotational energy,

$$E_{\mathrm{rot}} = \tfrac{1}{2}I_{\mathrm{ps}}|\vec{\omega}|^2, \tag{3}$$

of each jump. I_{ps} is the moment of inertia of the Platonic solid for rotations about any axis that contains the center of mass. Since the inertia tensor is a sphere, we do not need to distinguish the different rotational degrees of freedom (DOFs) but treat them as equivalent and evaluate their sum only.

III. RESULTS

A. Energy distributions

A characteristic property of particles excited by a vibrating plate is the probability density of energies in different DOFs, e.g., $p(E_z)$ and $p(E_{\rm rot})$, where in the gravitational field E_z is the sum of the potential energy and the kinetic energy of the vertical motion. In the absence of gravity, it represents the kinetic energy in the translational degree of freedom normal to the wall. Investigations on a single sphere [24] on a vibrating plate showed that the distribution $p(E_z)$ of a jump with the energy E_z can be described by

$$p(E_z) \propto E_z^{\frac{(1-\gamma)}{2(1+\gamma)}} \exp\left[\frac{4(\gamma-1)E_z}{(1+\gamma)^2 mV_{\rm pl}^2}\right], \qquad (4)$$

where γ is the restitution coefficient. When the jumps become ideally elastic ($\gamma \to 1$), a Boltzmann distribution is approached. This probability density can be used for a straightforward calculation of the mean kinetic energy $\langle E_z \rangle$ per jump. Note, however, that this value is not equivalent to the time-averaged energy $\langle E_z \rangle_t$: Higher jumps enter the time average with a higher statistical weight because their duration is longer.

In experiments with a rod on a vibrating plate [28], it was found that $p(E_z)$ can be roughly approximated by

$$p(E_z) \propto E_z^2 \exp\left(-\frac{E_z}{E_0}\right). \qquad (5)$$

In our current experiments, we find a clearly different situation; see Fig. 2. For all excitation schemes, we observe peaks in the distributions $p(E_z)$ and $p(v_0)$. This means that $p(E_z)$ cannot be described by a simple exponential relation like that in Eq. (5). A comparison between the cube and icosahedron experiments shows that higher energy jumps are more likely for the icosahedron than for the cube at the same excitation.

Since E_z and v_0 are directly related to the jump time t_j [see Eqs. (1) and (2)], it seems reasonable to compare the most probable jump durations (peaks in E_z) with the excitation period of the vibrating plate. Figure 2 (bottom) shows the distribution $p(t_j/T_{\rm pl})$ with the jump time t_j normalized by the excitation period $T_{\rm pl} = 1/f_{\rm pl}$ at 20 Hz excitation. The most probable jump times [peaks in $p(E_z)$, $p(v_0)$, and $p(t_j/T_{\rm pl})$] are located around integer multiples of the excitation period $T_{\rm pl}$ for all investigated frequencies $f_{\rm pl}$. The reason for this synchronization trend is probably found in the comparably low vibration frequency of the ground plate and the relatively low jump heights. Both conditions are related to technical limitations of the experiment: In comparison to earlier studies, (e.g., [28]), the bodies are much heavier and the achieved jump heights h_j are moderate, so that the flight times $t_j = \sqrt{8gh_j}$ of the individual jumps are of the same order of magnitude as the excitation period. Technically, the particle sizes and masses could not be reduced because of the restrictions set by the board inside. Increasing $f_{\rm pl}$ would not help either since the efficiency of excitation goes down with increasing $f_{\rm pl}$ due to limitations of the available shaker to a maximum Γ.

In contrast to experiments with a sphere on a vibrating plate, the rotational DOFs of the Platonic solids are directly excited during the frictional contacts with the plate. The three

TABLE III. Fit parameter $\langle E_{\rm rot} \rangle$ and amount of jumps with at least one saturated rotational component (Sat.) for all experiments. Values in parentheses are underestimated because of the gyroscope limits.

	Cube		Icosahedron	
$f_{\rm pl}$	$\langle E_{\rm rot} \rangle$ [mJ]	Sat. [%]	$\langle E_{\rm rot} \rangle$ [mJ]	Sat. [%]
20	(1.39)	22.80	(1.29)	25.5
30	0.77	7.20	0.84	11.4
40	0.53	1.00	0.52	2.6
50	0.31	0.10	0.29	0.25

individual rotational degrees of freedom are recorded individually by the gyroscopes, yet we did not treat the components of $\vec{\omega}$ separately but evaluated only the amount, the scalar ω. Since the inertia tensors of the Platonic solids are spherically symmetric with three equal eigenvalues, there is no distinguished axis for rotations. The angular momentum is always in the direction of $\vec{\omega}$. The rotation axis is conserved until the next collision with the ground plate. This is confirmed by the gyroscope data. When comparing rotations and translations, we have to keep in mind that the rotational energy is the sum of the contributions of three rotational DOFs.

The probability density distribution $p(E_{\rm rot})$ has an appearance that differs qualitatively from that of the translational motion. In Fig. 3 the probability density functions $p(E_{\rm rot})$ for the cube and the icosahedron at an excitation with $f_{\rm pl} = 30$ Hz is shown. The probability density can be described reasonably well by a Boltzmann distribution

$$p(E_{\rm rot}) = \frac{1}{\langle E_{\rm rot} \rangle} \exp\left(-\frac{E_{\rm rot}}{\langle E_{\rm rot} \rangle}\right). \qquad (6)$$

The fit parameter $\langle E_{\rm rot} \rangle$ represents the mean rotational energy. It is given in Table III for both shapes and all excitation parameters. One problem of the MMCs is the limited range of the gyroscope. Depending on the excitation parameters one or more of the measured gyroscope axes may occasionally be saturated. Thus some of the measured values for $E_{\rm rot}$ appear smaller than they are. This is especially the case for the 20 Hz gyroscope data. In Table III the percentage of $E_{\rm rot}$ values with at least one saturated rotation axis is shown. The maximum detectable rotational energy is about 4.5 mJ per jump for both Platonic solids. In the distributions $p(E_{\rm rot})$ for 20 Hz and 30 Hz excitation we found slight peaks around 1.5 mJ. These peaks seem to be measurement artifacts caused by this saturation effect. They vanish if we calculate the distribution only from unsaturated values of $E_{\rm rot}$. For 40 Hz and 50 Hz excitation, the peaks are not present because of the negligibly small number of saturated $E_{\rm rot}$ values. The reason for the decreasing mean energy at higher excitation frequencies is that the maximum plate velocity, and not the maximum plate acceleration, plays the decisive role for the excitation. When Γ is kept constant, higher vibration frequencies correspond to a reduced $V_{\rm pl}$ (Table I) and thus to less efficient excitation.

B. Correlations of energy data

An interesting aspect is the question of whether energies in subsequent jumps are correlated with each other. Naturally,
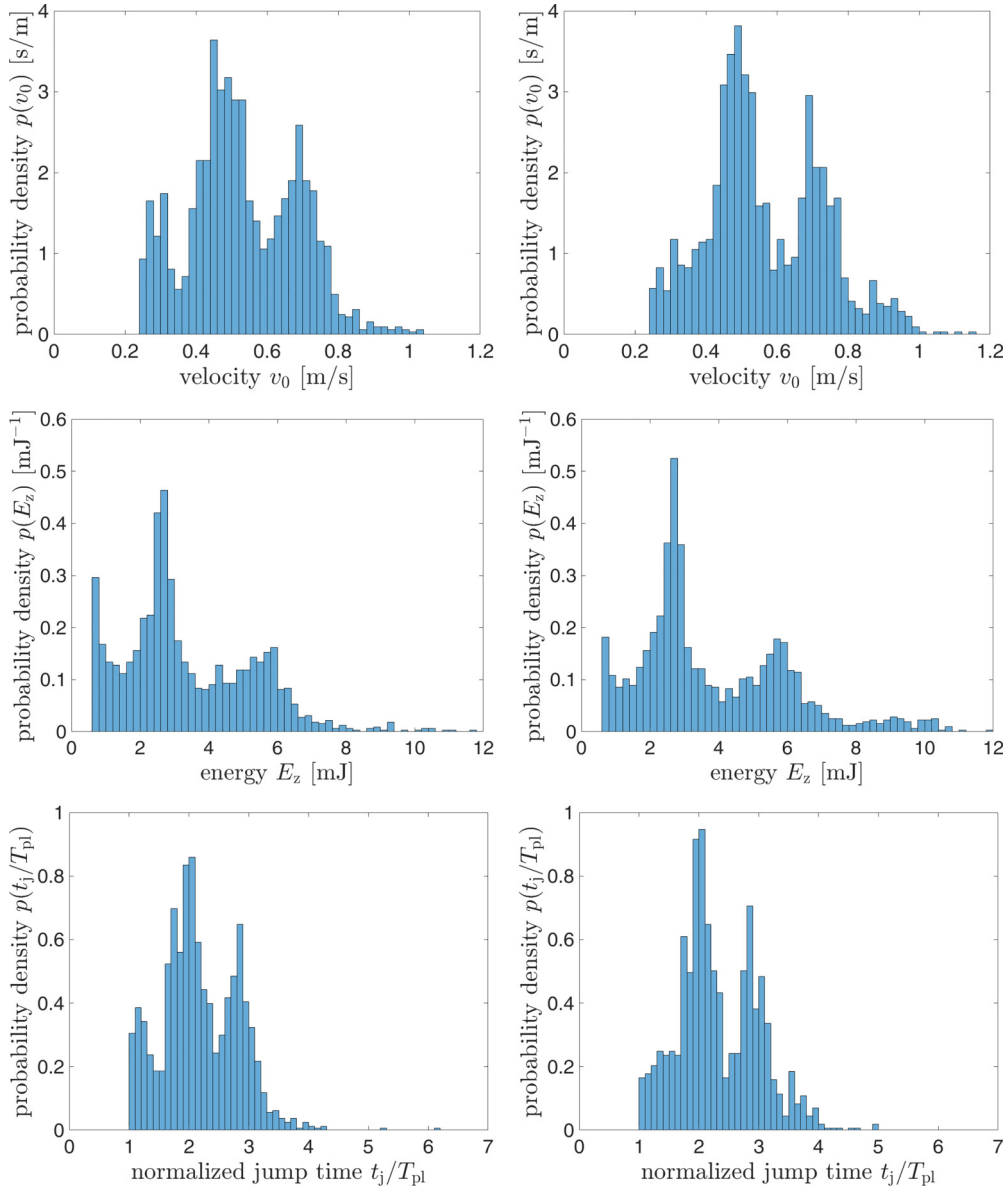
FIG. 2. Probability density of the velocity v_0 (top), the energy E_z (middle), and the normalized jump time t_j/T_{pl} (bottom) for an excitation with $f = 20$ Hz and $A = 3.1$ mm. The left column shows the distributions for the cube and the right column for the icosahedron. The velocity distributions $p(v_0)$ and energy distributions $p(E_z)$ clearly show peaks at similar energies for both Platonic solids. For the cube, low energy jumps (lower jumps) are more common than for the icosahedron. The corresponding distributions $p(t_j/T_{pl})$ for the cube and the icosahedron (same data as in the graphs above) show peaks that are located near integer multiples of the excitation period. Jumps shorter than $t_j/T_{pl} = 1$ are treated as double collisions and ignored here.

one might assume that a jump with high altitude and thus higher energy is also followed by a jump with an above-average energy. In order to analyze this problem, we have calculated the correlations between the nth and $(n + 1)$-st jumps. Figure 4 shows the correlations of the energy in the vertical degree of freedom (potential plus kinetic) in successive jumps. Each box shows the probability of a jump n with energy $E_z(n)$ followed by the next jump with energy $E_z(n + 1)$. The graphs on the left show the experimental data, while on the right we show the pattern that would result from completely uncorrelated jumps with the probability densities $p(E_z)$ similar to those shown in Fig. 2. The upper images

represent the cube, the lower two images are those of the icosahedron. Within statistical error, the plots are nearly identical. Thus, we can conclude that there is no significant global correlation between the heights of successive jumps. With regard to the mechanical excitation of grains in a granular ensemble this means that a "hot" particle practically does not have a higher probability than a "colder" one to leave the exciting plate with a high translational kinetic energy. Note that this is significantly different from collisions with a static wall where the faster particle always remains faster after reflection. With the peak velocity of the wall being of the same order as that of the bouncing particle, the kinetic states of the
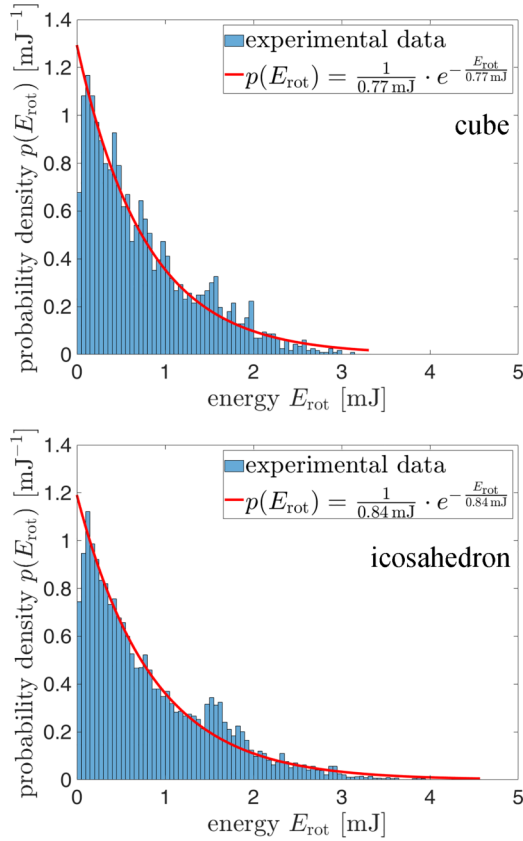
FIG. 3. Probability density distribution $p(E_{\mathrm{rot}})$ for the cube (top) and the icosahedron (bottom) at an excitation with $f = 30$ Hz and $A = 1.6$ mm. The distributions almost coincide for both bodies. Jumps with energies of $E_{\mathrm{rot}} \approx 1.5$ mJ are slightly overpronounced in the experimental data compared to the empirical fit (red solid line) for both cases. The functional form of the fit can be found in the insets.

latter are strongly mixed because of the different phases of the plate motion at impact. Some correlations may exist on a small scale, which are not resolved in the crude grid structure of our plots. The box size was a compromise of sufficient statistical data in each box and reasonable energy resolution.

There appears to be just a marginal overpopulation of the boxes near the diagonal, i.e., the probability that a certain jump is followed by a jump of comparable height is slightly more probable than consecutive jumps of very different heights.

A similar statistics is shown for the correlations of the translational energy E_z and the rotational energy E_{rot} in individual jumps in Fig. 5 in order to find out whether larger rotational energies are correlated with a reduced jump height or kinetic energy of the vertical motion. Again, the left-hand side shows the experimental result, the right-hand side the product of the respective probability densities, representing the prediction for totally uncorrelated quantities. As one can see, there is also no significant correlation. For each column (given E_z), the rotational energies are distributed with the same weights as shown in Fig. 3. Within statistical uncertainty, the rotational and translational energies in individual jumps are uncorrelated.

C. Mean energy transfer

An important characteristics of our experiments, relevant for the application of vibrating walls for the excitation of granular gases, are the mean energies ($\langle E_z \rangle$, $\langle E_{\mathrm{rot}} \rangle$, $\langle E_{\mathrm{tot}} \rangle$) transferred to the bouncing objects. In addition to the experimental results we show simulation data, obtained by a numerical approach described in [42]. The simulated bodies had the same masses m and the same moments of inertia I_{ps} as the experimental ones. The chosen restitution coefficient was $\gamma = 0.8$. In contrast to the results presented in [42], we define a jump as the time between two consecutive plate contacts, and not as the time between sign changes of the vertical velocity. This minor detail does not influence the general outcome of the simulations. Similar to the experiments we neglected jumps that are shorter than T_{pl}, which can be considered as double contacts. Such collisions occur when the Platonic solid hits the vibrating plate with one corner first and then makes another contact immediately after with another corner. Such double contacts were described earlier for rods on a vibrating plate [28].

In the simulations, the energy of translations in the horizontal plane E_{xy} is accessible in addition. This quantity is difficult to retrieve with our observation technique from the sensor data, because they provide only accelerations. A numerical integration is in principle possible but requires complex mathematical efforts (because of the concurrent rotations) and would lead to large uncertainties in the obtained in-plane velocities. The energy E_{xy} obtained from the simulations is on average small compared to the energy in the vertical translational motion. It is about $0.1 \langle E_{\mathrm{tot}} \rangle$ for the cube and about $0.15 \langle E_{\mathrm{tot}} \rangle$ for the icosahedron. For compatibility with the experiment, we neglect it in the calculation of $E_{\mathrm{tot}} = E_z + E_{\mathrm{rot}}$ (as in the experiment).

In Fig. 6 the dependence of the mean energies $\langle E_* \rangle$ on the plate frequency at $\Gamma = 5\,g$ is shown (the asterisk symbol stands for "rot," "z," and "tot"). There is an acceptable agreement of the mean energy values $\langle E_* \rangle$ between experiment and simulation for the plate frequencies $f_{\mathrm{pl}} \geqslant 30$ Hz. We have to keep in mind that about 25% of the E_{rot} values were clipped by the limited measurement range at 20 Hz excitation. Thus, the measured experimental mean energies $\langle E_{\mathrm{rot}} \rangle$ are somewhat smaller than their actual values. For 20 Hz the simulation delivers a more effective excitation than the experiment especially for $\langle E_z \rangle$. However, one can reproduce the experimental values for $\langle E_z \rangle$ reasonably well by using a somewhat lower restitution coefficient of $\gamma = 0.7$ in the simulation of the 20 Hz experiment. It is clearly visible that all quantities $\langle E_* \rangle$ decrease with increasing frequency, so a higher frequency (lower V_{pl}) leads to a less effective excitation. This behavior is found both in the experiments and in the simulations. The explanation was given in the previous section. The total energy decay can roughly be approximated by power laws $f_{\mathrm{pl}}^{-\beta}$ with exponents β in the range 1.8 ± 0.3.

While the frequency parameter is only of secondary importance for the bouncing dynamics, the plate velocity is of primary interest. The dependence of the mean energies $\langle E_* \rangle$ on the maximum plate velocity V_{pl} is shown in Fig. 7. For a sphere on a vibrating plate, $\langle E_z \rangle$ would be proportional to V_{pl}^2 for sufficiently large jump heights [23–26]. For other objects
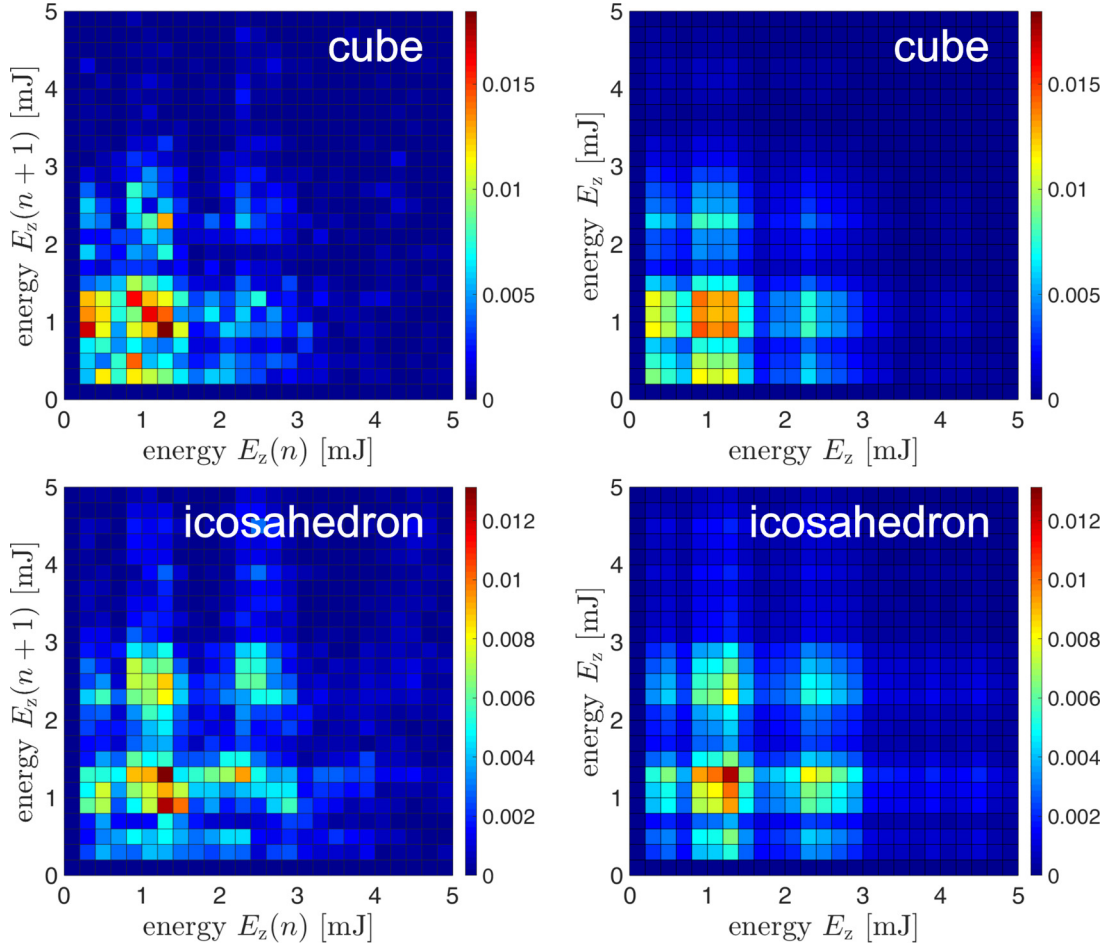
FIG. 4. Correlation between the translational energy E_z of the (n)th jump and of the ($n+1$)-st jump at an excitation with 30 Hz. The top row shows the data for the cube and and the bottom row the data for the icosahedron. In both cases we do not find a significant correlation. Explanation is given in the text. Left: experimental results, right: distribution under the assumption of totally uncorrelated energies, just showing the product of the energy distribution densities.

like rods, $\langle E_{\text{tot}} \rangle \propto V_{\text{pl}}^{1.4}$ [28], or tetrahedrons, $\langle E_* \rangle \propto V_{\text{pl}}^{1.6}$ [42], the exponents were found to be significantly smaller. In the present case, all quantities $\langle E_* \rangle$ can be approximated by

$$\langle E_* \rangle \propto V_{\text{pl}}^{\alpha}, \qquad (7)$$

but the fitted exponents α differ considerably. In particular, there are discrepancies between experimental and simulated data; see Fig. 7 and Table IV.

One reason for the quite small exponents at 20 Hz excitation in the experiment is that the clipped angular velocity data lead to an underestimation of the rotational energy at that low frequency. A larger rotational energy at 20 Hz (by

TABLE IV. Fitted exponents α of the relation $\langle E_* \rangle \propto V_{\text{pl}}^{\alpha}$ for experimental and simulated data. Corresponding fit curves are shown in Fig. 7. The uncertainty of these values is ± 0.3.

	Experiment			Simulation		
	E_{rot}	E_z	E_{tot}	E_{rot}	E_z	E_{tot}
Cube	1.4	1.9	1.7	1.5	2.0	1.9
Icosahedron	1.3	1.7	1.6	1.5	1.9	1.8

about 20%) would raise the fitted exponent of E_{rot} to ≈ 1.7. The establishment of the plate velocity dependence was not the primary focus of our study. A more accurate determination of the exponents would require a larger frequency range and stronger excitations, which were not available for this study. In particular, one has to be aware that the frequency or plate velocity dependence of the excitation at constant maximum acceleration may not give the complete answer, because the mean energies may depend in a more complex manner on both amplitude and frequency of the plate vibrations.

D. Energy ratios

Figure 8 shows how the mean energies are distributed among the different DOFs in the experiment. In Fig. 8 (top), the ratio $\langle E_{\text{rot}} \rangle / \langle E_{\text{tot}} \rangle$ is presented. The share of rotational energy is roughly about 32% for the cube and somewhat smaller for the icosahedron ($\approx 27\%$). At 50 Hz excitation, the share of rotational energy shows a slight drop for the cube. The explanation is that at this frequency, the plate velocity and thus the efficiency of the excitation is already quite low. and the jump heights are comparable to the side lengths of the bodies. The mean jump heights at 50 Hz excitation are 2.9 mm
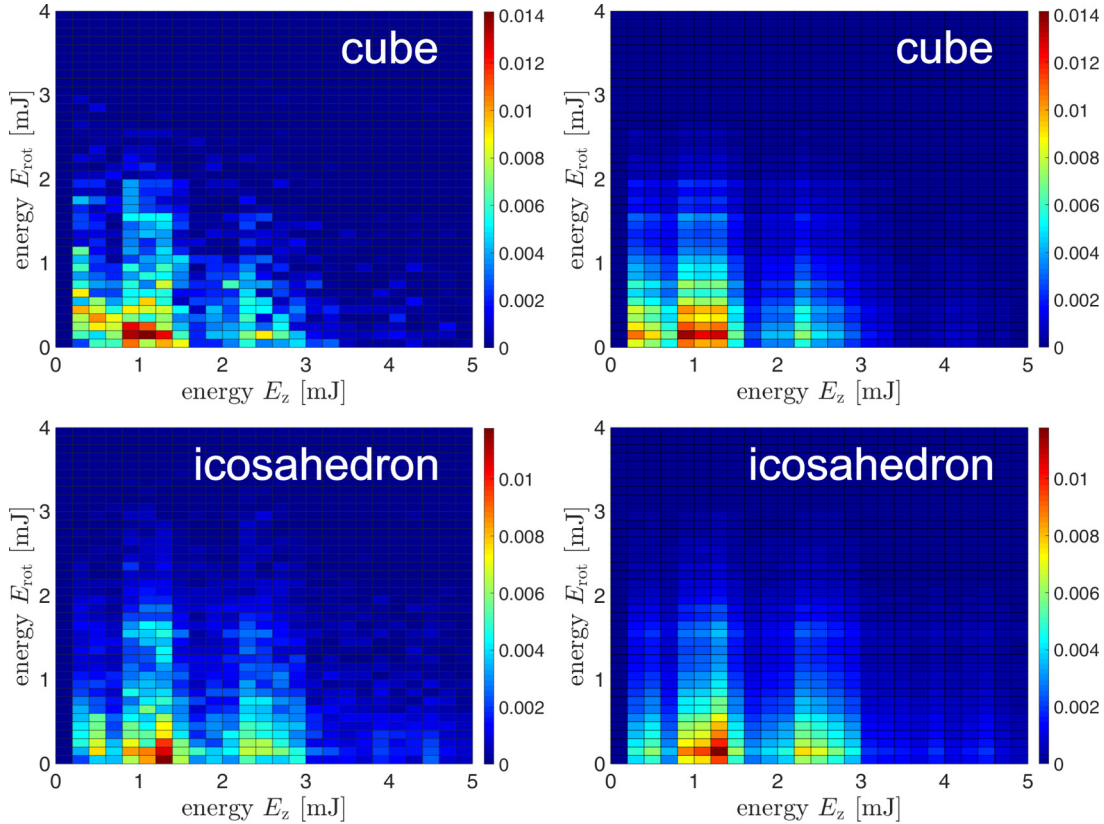
FIG. 5. Correlation between the rotational energy E_{rot} of the (n)th jump and the translational energy E_z of the same jump at an excitation with 30 Hz. The top row shows the data for the cube and the bottom row the data for the icosahedron. For both bodies we do not find a significant correlation. Left: experimental results; right: distribution under the assumption of totally uncorrelated energies, just showing the product of the energy distribution densities.

for the cube and 3.5 mm for the icosahedron. For the cube, about 90% of the jumps are lower than 5.4 mm, which is the necessary level for a rotation of the cube over an edge. In this situation, flips across edges with a change of the downward face of the cube are strongly hindered, so that torques of consecutive collisions with the plate partly compensate each other. This problem is slightly less acute for the icosahedron, with its shape being closer to a sphere.

In Fig. 8 (bottom), the ratios of the kinetic energies $\langle E_*^{\text{cub}}\rangle/\langle E_*^{\text{ico}}\rangle$ between cube and icosahedron at the same excitation conditions are shown. Within the experimental error, the ratios are almost constant. The amount of transferred rotational energy is almost equal for both Platonic solids, while the transferred amount of energy in the z direction for the cube is only $\approx 80\%$ of the energy $\langle E_z^{\text{ico}}\rangle$ of the icosahedron. For the total transferred energy, a ratio of $\langle E_{\text{tot}}^{\text{cub}}\rangle/\langle E_{\text{tot}}^{\text{ico}}\rangle \approx 85\%$ is found. The excitation of translational motions with the same parameters is noticeably more efficient for the icosahedron.

IV. DISCUSSION

We have employed an experimental technique to record information on the motion of jumping Platonic solids by equipping these objects with autonomous IMUs. The storage of acceleration and rotation data makes the statistical analysis of the jump dynamics much less time consuming than the standard technique based on optical video data. In particu-

lar, rotations are much more easily extracted from the IMU records. This technique may also become an useful substitute, or at least a strong complement, for the optical observation of granular gases under microgravity conditions in 3D experiments. One may use much denser ensembles (higher particle number densities) than in experiments using optical observation, since background particles are not obscured by others in the optical path. Also, the extraction of rotational motion is much easier to achieve. Collision rates are easily detected too.

One of the restrictions of the IMUs used in this study is the limited measurement range of the gyroscopes. This can be circumvented when only a moderate excitation strength is used. For the highly symmetric bodies studied here, all rotations about the center of mass are equivalent, thus we did not distinguish between individual rotational DOFs, but treat them as equivalent. Our rotational energy data represent the sum of these three DOFs.

The velocities of the particles can in principle be calculated from the integration of acceleration data, employing the rotation data and quaternions. In the present study, this was not necessary since the objects are in free fall between the collisions and the translational motion is analytically known.

The main result of this study is the comparison of energy partition between translational and rotational degrees of freedom, which is an important issue when vibrating container walls are used to heat up granular gases in microgravity. It turns out that the rotations are excited by nearly one order of
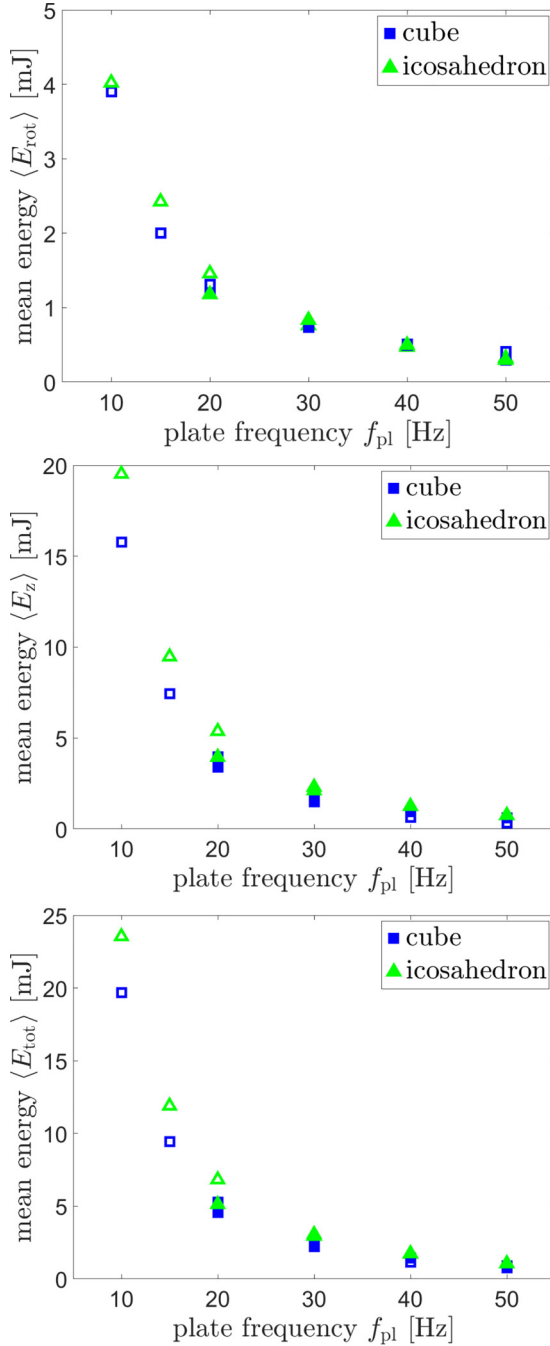
FIG. 6. Mean energies $E_*(f_{pl})$ for the simulated (open symbols) and experimental data (filled symbols) at constant plate acceleration $\Gamma = 5\,g$. For both Platonic solids all mean energies $\langle E_* \rangle$ decrease with increasing plate frequency f_{pl}. For the simulations, a restitution coefficient of $\gamma = 0.8$ was used.

FIG. 7. Dependence of the mean kinetic energies $\langle E_* \rangle$ on the plate velocity amplitude V_{pl}. Filled symbols show experimental data and open symbols simulated data ($\gamma = 0.8$). The lines are fits of the data with $\langle E_* \rangle \propto V_{pl}^{\alpha}$; see text. Solid lines belong to experimental data and dashed ones to the simulations. The corresponding excitation frequencies $f_{pl} = 5g/(2\pi V_{pl})$ are marked in the top image.

magnitude less than the vertical translational degree of freedom. All three rotational degrees of freedom together reach less than one third of the total kinetic energy. An additional observation is that the share of the excitation of rotations is not substantially different between the cube and the icosahedron, even though the icosahedron shape is much closer to that of a sphere, where ideally rotations are not excited at all.
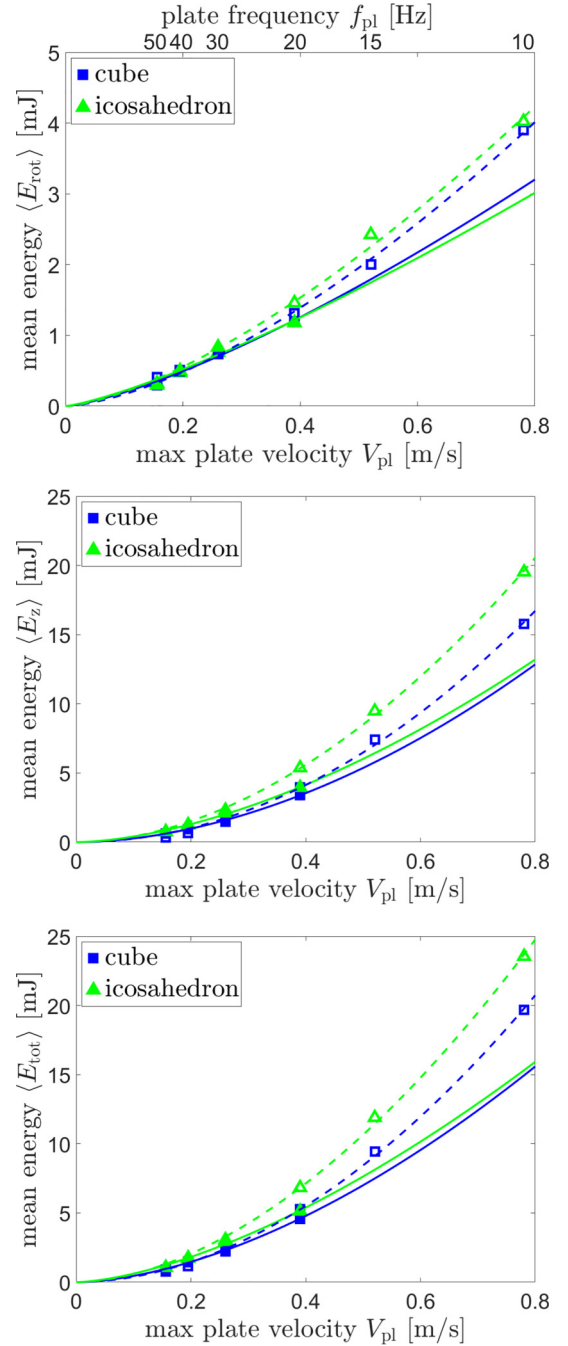
Our investigation could easily be extended to octahedra and dodecahedra, yet we do not expect qualitatively new results. The geometrical parameters derived in the Appendix suggest that they will behave very similar to the cube and the icosahedron, respectively. In view of the small differences between cube and icosahedron, similar values for the two other polyhedra can be expected. In addition to the methodical
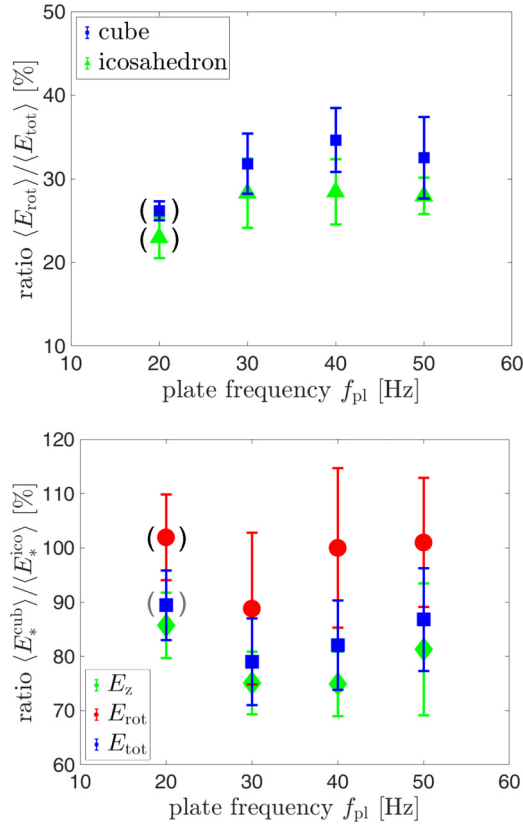
FIG. 8. Top: amount of rotational energy on the total energy for both Platonic solids; bottom: ratios of the different kinetic energies $\langle E_*^{\text{cub}} \rangle / \langle E_*^{\text{ico}} \rangle$ of the two Platonic solids at the same excitation parameters. Data in parentheses are affected by the partially clipped rotational velocity data.

development and the statistical evaluation of experiments, we have obtained some results of numerical simulations based on a DEM code (YADE) [42] and compared them with the experimental data. These simulations support the conclusion that octahedra and dodecahedra show comparable energy partitions as the polyhedra investigated here.

A remark concerning the edges and vertices of the polyhedra seems appropriate here. While in jumps of ellipsoids and spheres this problem does not exist, the contacts of polyhedra with the vibrating plate occur almost exclusively at their vertices, very rarely with edges. Since these structures are not infinitely sharp in the experiment, the influence of rounded vertices was tested in the numerical simulations. It was found that rounded edges and vertices with radii of curvature not exceeding 1 mm (less than 5% of the edge lengths) had only minimal impact on the results. The experimental vertices and edges were much sharper, thus the experimental results can be regarded as robust.

We also analyzed the correlations between the rotational and translational energies within the individual jumps, and correlations of energies of subsequent jumps. We did not find statistically relevant correlations between the translational energies in subsequent jumps. This evidences that the excitation parameters used mix the dynamic states of the jumping object very well. Neither did we observe a correlation between the translational and rotational energy shares within

individual jumps. This is an indication that the amount of energy transferred into rotations or regained from rotations during collisions does not noticeably influence the energy contained in the vertical translational motion.

It may be appropriate to emphasize that the results are valid independent of the particle sizes. The geometrical and mechanical quantities relevant in the present experiment have different dependencies on the side length a of the polyhedra: While the mass m is related to the third power of the side length, a^3, the moment of inertia scales with a^5. The mean velocities and jump heights remain practically unchanged because they depend solely on the plate motion and the restitution coefficient. Thus the translational energy scales with a^3 via the mass, while rotational energy depends upon the moment of inertia I and the square of the rotation frequency ω. It remains to be shown that under these conditions the ratio of the kinetic energies does not depend upon a.

The reasoning is as follows. The torques scale with a^4 via the mass m and the length ℓ. Angular velocities ω, which involve the torques and the moment of inertia, will scale with $1/a$. The kinetic energy of rotations $I\omega^2/2$ will therefore also scale with a^3, as the translational energies. As expected, all ratios of the mean energies in the individual degrees of freedom are independent of the size of the objects. The only change is the slowing of rotations with increasing edge lengths a. This will change the relations between ω and the vibration frequency f_{pl} of the plate, with consequences for the details of the particle trajectories.

A. Summary

In our study we measured the dynamics of two representative Platonic solids (cube and icosahedron) excited by a vibrating plate. The results can be summarized as follows:

(1) Rotations of the two investigated particle shapes are much less excited than the vertical translational motion (Figs. 6 and 8).

(2) Even though the deviation from sphere shape is much larger for the regular hexahedron (six faces, eight vertices) than for the icosahedron (20 faces, 12 vertices), there is only a little difference in the energy partition. Within the statistical uncertainty, these solids behave similarly (Fig. 6).

(3) The energy distribution of rotational energies follows an exponential decay (Fig. 3). The authors are not aware of comparable results in the literature or theoretical work that predicted this behavior. For translational motions of spheres, the kinetic energy distribution follows a completely different scheme [24].

(4) The observation that energies in successive jumps are only weakly correlated is not trivial. Naturally, one might have expected that a particle impacting at high speed on the vibrating plate would also leave the plate on average with larger speed than a slowly impacting body. This is clearly not the case in our experiments.

One may extend the proposed observation technique easily to less symmetric particles such as ellipsoids or cylinders (oblate or prolate). In general, the inertia tensor will not be symmetric anymore, and thus one has to distinguish three different rotational degrees of freedom. This is not a problem because the IMU provides separate information on the

individual rotational DOFs. Nevertheless, it seems that the comparably weak excitation of rotational degrees of freedom, which was also reported for the "extreme" case of thin rods [28], is a general feature of mechanical excitation with vibrating plates.

APPENDIX: ENERGY TRANSFER IN ELASTIC COLLISIONS

We assume that a nonrotating solid object hits a plate at rest with a velocity v_1, perpendicular to the plate. It will have the moment of inertia I, with a spherically symmetric inertia tensor, and a mass m. The distance from the vertical through the center of mass and the contact point will be ℓ. After the collision, the velocity is v_2 and the angular velocity becomes ω_2. The normal force $F(t)$ at the contact point generates a torque $\ell F(t)$. Then the momentum equation reads

$$m(v_2 - v_1) = \int F\,dt, \qquad (A1)$$

where the integral is over the contact time and the contact point is assumed to be fixed (no sliding). For the angular momentum, one has

$$I\omega_2 = \ell \int F\,dt. \qquad (A2)$$

The combination of these equations yields

$$\omega_2 = \frac{m\ell}{I}(v_2 - v_1). \qquad (A3)$$

TABLE V. Optimal distance of the contact point ℓ_{opt} for the excitation of rotations and maximum possible distance R_{F} in units of the edge length and their ratio.

Body	ℓ_{opt}/a	R_{F}/a	$\ell_{\text{opt}}/R_{\text{F}}$
Tetrahedron	0.224	0.577	0.388
Cube	0.408	0.707	0.577
Octahedron	0.316	0.577	0.547
Dodecahedron	0.779	0.851	0.916
Icosahedron	0.511	0.577	0.885

Inserting this relation into the kinetic energy balance

$$\frac{m}{2}\left(v_1^2 - v_2^2\right) = \frac{I}{2}\omega^2, \qquad (A4)$$

and introducing a reduced length $\lambda = \sqrt{m/I}\,\ell$ one obtains the quadratic equation

$$v_1^2(1 - \lambda^2) - v_2(1 + \lambda^2) + 2\lambda^2 v_1 v_2 = 0 \qquad (A5)$$

with one physically relevant solution

$$v_2 = \frac{\lambda^2 - 1}{\lambda^2 + 1}v_1, \quad \omega_2 = \frac{-2\lambda}{\lambda^2 + 1}\sqrt{\frac{m}{I}}v_1. \qquad (A6)$$

The related rotational energy after the collision is

$$E_{\text{rot}} = \frac{2\lambda^2}{(1 + \lambda^2)^2}mv_1^2, \qquad (A7)$$

which achieves its maximum at $\lambda_{\text{opt}} = 1$, that is,

$$\ell_{\text{opt}} = \sqrt{I/m}. \qquad (A8)$$

When the distance ℓ is equal to that value, the maximum rotational energy is gained by an initially nonrotating object bouncing on a plate at normal impact. For the five Platonic solids, the optimum distances are listed in Table V.

Of course, these considerations yield only a crude approximation of the efficiency of torques on Platonic solids. When the body is rotating before the collision, the computation contains many more parameters and requires a much more detailed analysis. In addition, a restitution coefficient <1 will change the result. Nevertheless, the simplified model gives a rough indication what rotational energies can be expected for the different Platonic solids.

[1] H. M. Jaeger, S. R. Nagel, and R. P. Behringer, Rev. Mod. Phys. **68**, 1259 (1996).

[2] S. Luding, E. Clément, A. Blumen, J. Rajchenbach, and J. Duran, Phys. Rev. E **49**, 1634 (1994).

[3] E. Falcon, R. Wunenburger, P. Evesque, S. Fauve, C. Chabot, Y. Garrabos, and D. Beysens, Phys. Rev. Lett. **83**, 440 (1999).

[4] E. Falcon, S. Aumaitre, P. Evesque, F. Palencia, C. Lecoutre-Chabot, S. Fauve, D. Beysens, and Y. Garrabos, Europhys. Lett. **74**, 830 (2006).

[5] H.-Q. Wang, K. Feitosa, and N. Menon, Phys. Rev. E **80**, 060304(R) (2009).

[6] K. Harth, T. Trittel, S. Wegner, and R. Stannarius, EPJ Web Conf. **140**, 04008 (2017).

[7] M. Noirhomme, F. Ludewig, N. Vandewalle, and E. Opsomer, Phys. Rev. E **95**, 022905 (2017).

[8] M. Noirhomme, A. Cazaubiel, E. Falcon, D. Fischer, Y. Garrabos, C. Lecoutre-Chabot, S. Mawet, E. Opsomer, F. Palencia, S. Pillitteri, and N. Vandewalle, Phys. Rev. Lett. **126**, 128002 (2021).

[9] D. Puzyrev, D. Fischer, K. Harth, T. Trittel, R. C. Hidalgo, E. Falcon, M. Noirhomme, E. Opsomer, N. Vandewalle, Y. Garrabos *et al.*, Sci. Rep. **11**, 10621 (2021).

[10] K. Harth, U. Kornek, T. Trittel, U. Strachauer, S. Höme, K. Will, and R. Stannarius, Phys. Rev. Lett. **110**, 144102 (2013).

[11] T. Poeschel and S. Luding (eds.), *Granular Gases* (Springer, Berlin, 2001).

[12] K. Feitosa and N. Menon, Phys. Rev. Lett. **88**, 198301 (2002).

[13] K. Feitosa and N. Menon, Phys. Rev. Lett. **92**, 164301 (2004).

[14] K.-C. Chen, C.-H. Lin, C.-C. Li, and J.-J. Li, J. Phys. Soc. Jpn. **78**, 044401 (2009).

[15] H. Uecker, W. T. Kranz, T. Aspelmeier, and A. Zippelius, Phys. Rev. E **80**, 041303 (2009).

[16] J. Wakou and M. Isobe, Phys. Rev. E **85**, 061311 (2012).

[17] C. R. K. Windows-Yule and D. J. Parker, Phys. Rev. E **87**, 022211 (2013).

[18] K. Harth, T. Trittel, K. May, S. Wegner, and R. Stannarius, Adv. Space Res. **55**, 1901 (2015).

[19] Y. Chen, P. Evesque, and M. Hou, Eng. Computations **32**, 1066 (2015).

[20] S. M. Rubio-Largo, F. Alonso-Marroquin, T. Weinhart, S. Luding, and R. C. Hidalgo, Physica A **443**, 477 (2016).

[21] G. Castillo, S. Merminod, E. Falcon, and M. Berhanu, Phys. Rev. E **101**, 032903 (2020).

[22] R. D. Wildman and D. J. Parker, Phys. Rev. Lett. **88**, 064301 (2002).

[23] S. Warr, J. M. Huntley, and G. T. H. Jacques, Phys. Rev. E **52**, 5583 (1995).

[24] S. Warr, W. Cooke, R. C. Ball, and J. M. Huntley, Physica A **231**, 551 (1996).

[25] J.-C. Geminard and C. Laroche, Phys. Rev. E **68**, 031305 (2003).

[26] J.-Y. Chastaing, E. Bertin, and J.-C. Géminard, Am. J. Phys. **83**, 518 (2015).

[27] H. S. Wright, M. R. Swift, and P. J. King, Phys. Rev. E **74**, 061309 (2006).

[28] T. Trittel, K. Harth, and R. Stannarius, Phys. Rev. E **95**, 062904 (2017).

[29] G. M. Zaslavski, Phys. Lett. A **69**, 145 (1978).

[30] P. J. Holmes, J. Sound Vib. **84**, 173 (1982).

[31] P. Pierański, J. Phys. France **44**, 573 (1983).

[32] Z. J. Kowalik, M. Franaszek, and P. Pieranski, Phys. Rev. A **37**, 4016 (1988).

[33] J. M. Luck and A. Mehta, Phys. Rev. E **48**, 3988 (1993).

[34] N. B. Tufillaro, Phys. Rev. E **50**, 4509 (1994).

[35] S. Vogel and S. J. Linz, Int. J. Bifurcation Chaos **21**, 869 (2011).

[36] J. Atwell and J. S. Olafsen, Phys. Rev. E **71**, 062301 (2005).

[37] S. Dorbolo, D. Volfson, L. Tsimring, and A. Kudrolli, Phys. Rev. Lett. **95**, 044101 (2005).

[38] S. Dorbolo, F. Ludewig, and N. Vandewalle, New J. Phys. **11**, 033016 (2009).

[39] R. D. Wildman, J. Beecham, and T. L. Freeman, Eur. Phys. J. Spec. Top. ST **179**, 5 (2009).

[40] J. Wang, C. Liu, and D. Ma, Proc. Roy. Soc. A **470**, 20140439 (2014).

[41] J. Wang, C. Liu, M. Wiercigroch, C. Wang, and Y. Shui, Nonlinear Dyn. **86**, 1477 (2016).

[42] N. Dieckmann, D. Puzyrev, T. Trittel, and R. Stannarius, Ann. Phys. (Berl.) **536**, 2300349 (2023).